NIPPON STEEL TECHNICAL REPORT No. 91 JANUARY 2005

UDC 699 . 15' 295 : 621 . 785 . 53

Nitriding Behavior and Strengthening Mechanism of Ti-added Steels in Rapid Nitriding Process

Kazuhisa KUSUMI*1 Takehide SENUMA*2
Masaaki SUGIYAMA*3 Masayoshi SUEHIRO*2
Masako NOZAKI*4

Abstract

The nitriding process is one of the common methods for surface hardening, and consists of heat treatment in a furnace for many hours. The nitriding behavior and strengthening mechanism of Ti added steels in the nitriding process, which is applicable to a high temperature and rapid process such as the continuous annealing of steel strip, were investigated. Cold rolled Ti added steel sheets were annealed for recrystallization and nitrided in electric furnaces. Then the hardness distribution was measured in cross sections, and the sheets were found to strengthen only near the surfaces. The maximum hardness depended on the Ti content, and the thickness of hardened layer depended on the nitriding time and the flow rate of NH_3. Observation by means of electron microscopy showed contrasts due to fine disc particles with a size of 10nm in diameter and several atomic layers in thickness, which were considered to be Ti nitrides or Ti-N clusters. These contrasts were observed only near the surfaces. This suggests that the hardening is caused by the small particles. A diffusion model of N that considered the precipitation of TiN was used for simulating of the nitriding behavior. The result showed that N introduced into steel immediately precipitated as TiN, then supersaturated N diffused to the inside. The simulation result agrees with the experiment. The amount of strengthening was estimated. It indicated that the strengthening mechanism was mainly the precipitation hardening of Ti nitride or Ti-N clusters.

1. Introduction

The typical heat treatment methods employed for hardening steel surfaces include nitriding, carburizing and sulfurizing. Among these, nitriding is widely employed because of the advantages that the process temperature is comparatively low, approximately 550°C, and that the deformation such as thermal strain is small. Nitriding is a method for improving the wear resistance, seizing resistance, corrosion resistance and fatigue strength of steel material by hardening the surface layer by forming fine particles of iron nitride and/or the nitrides

*1 Yawata R&D Lab.
*2 Steel Research Laboratories
*3 Advanced Technology Research Laboratories
*4 Nippon Steel Technoresearch Corporation

of elements such as Cr, Al, Ti and Si in the surface layer [1]. The practices of nitriding include salt-bath soft nitriding, gas soft nitriding and ion nitriding, and all these methods usually require a long treatment time in a heat treatment furnace. Nitriding is applied generally to final products made of steel, and it has never been applied to material steel in a strip form.

In consideration of the latest requirements for strengthening of steel sheets for automobile use, the authors studied measures to improve the functionality of steel sheets for applications to the outer panels of an automobile body. One of the measures studied is the technology to apply nitriding to a steel strip in a short processing time on a continuous annealing line to harden the surface layers and enhance dent resistance without raising yield strength excessively. A dent is a local depression of an automobile body outer panel caused by a pressure applied from firm object [2], and dent resistance is improved usually by raising yield strength. However, formability deteriorates as yield strength increases, leading to problems typically such as surface deflection. In view of this, in order to improve dent resistance while avoiding the strengthening of a whole steel sheet, the authors conceived of increasing flexural rigidity by strengthening surface portions only using nitriding.

With respect to modification of surface layer material at high temperatures within a short process time of a continuous annealing line, some papers reported the behavior of steel materials at carburizing applied to improve bake-hardenability and the formability at secondary working [3]. However, there has been no paper at all either on the behavior of steel at nitriding or the mechanism of surface layer hardening by rapid nitriding at high temperatures. This paper reports the results of these studies into the hardness change in surface layers during rapid nitriding at high temperatures, and based on the results, into the behavior of steel at nitriding and the mechanism of the hardening.

2. Experimental Method

To examine the influence of Ti on the strengthening of surface layers, the authors used high-purity, ultra-low-C steels having different Ti contents as the specimen steels for the nitriding test, which was done by gas nitriding. **Table 1** shows the chemical compositions of the specimen steels. Ti remains in the state of solid solution in steel after hot rolling and plays an important role in nitriding; the amount of the solute Ti (Ti*) is obtained by subtracting the amount of Ti that precipitates as carbonitride and sulfide from the total amount of Ti. For the purpose of the present test it was defined as Ti* = 48 (N/14 + S/32 + C/12). Ingots of the specimen steels were rolled into cold-rolled sheets through the following processes: breakdown rolling to a thickness of 40 mm; machining to a size of 40 mm × 160 mm × 200 mm; heating to 1150°C; holding there for 1 h; hot rolling following a pass schedule from 40 through 24, 15, 9, 7 and 5 finally to 4 mm and at a finishing temperature of 900°C; coiling at 650°C; and cold rolling at a reduction ratio of 82.5% to a thickness of 0.7 mm. Cold-rolled sheets of a Ti-added ultra-low-C steel produced on commercial facilities were also used for observation of precipitates. The chemical composition of the steel is shown also in Table 1 as Steel D.

Recrystallization annealing and nitriding were carried out using two atmosphere-controllable electric furnaces arranged adjacent to each other. The recrystallization annealing was done in one of the furnaces for 60 s at 800°C in an inert atmosphere (25% N_2 + 75% H_2, flow rate 1.25 m/min), and thereafter, the specimens were quickly transferred to the other furnace for nitriding. The nitriding was done in an atmosphere prepared by mixing NH_3 to the above inert atmosphere. To examine the influence of the Ti addition amount, the Ti contents of Steels A, B and C were controlled to 0.016, 0.025 and 0.046 mass%, respectively, and the specimens were subjected to the nitriding for 20 and 40 s at a temperature of 750°C and a NH_3 flow rate of 0.05 m/min (NH_3 concentration 3.8%). To examine the influence of the NH_3 flow rate (NH_3 concentration), separate nitriding tests were conducted changing the flow rate from 0.025 to 0.5 m/min (NH_3 concentration from 2.0 to 28.6%), using Steel C and for a treatment time of 40 s. The heat patterns of the recrystallization annealing and nitriding are schematically shown in **Fig. 1**.

The amount of nitriding was measured by the inert gas fusion thermal conductivity method, and the sectional hardness distribution near the surfaces by the micro-Vickers hardness test under a load of 10 gf.

Precipitates were observed using electron microscopes with extraction replicas and thin film specimens prepared through electrolytic polishing. The specimens were prepared from the sheets of Steels C and D that underwent the nitriding for 40 s at 750°C and a NH_3 flow rate of 0.05 m/min (NH_3 concentration 3.8%). The electrolytic polishing was done by the jet polishing method using a solution of 95% acetic acid + 5% perchloric acid. The authors found that, as a phenomenon peculiar to nitride steel, a very thin oxide coating film having an Fe_2O_3 structure formed on the surfaces after such a polishing treatment, and this was taken into account in the analysis of electron beam diffraction patterns. The electron microscopes used for the tests were a JEM-200CX made by JOEL Ltd.

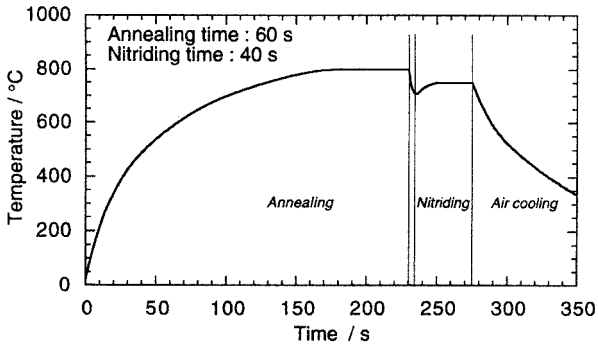

Fig. 1 Example of heat pattern in annealing and nitriding process

Table 1 Chemical composition of steels

(mass%)

	C	Mn	P	S	Al	N	Ti	Ti*
A	0.001	0.25	0.014	0.022	0.049	0.002	0.016	– 0.028
B	0.001	0.24	0.006	0.006	0.034	0.003	0.025	0.005
C	0.001	0.13	0.006	0.006	0.025	0.003	0.046	0.024
D	0.004	0.15	0.011	0.005	0.067	0.0025	0.060	0.030

and an HF-2000 made by Hitachi Ltd., which was equipped with a field emission type electron gun. Besides these, light-optic microscopes were used for the observation of metallographic structure.

3. Results

3.1 Influences of Ti amount and time and atmosphere of nitriding on surface layer hardening

The influences of the Ti addition amount and the nitriding time on the hardening of surface layers were investigated using Steels A, B and C. The metallographic structure was polygonal ferrite and the ferritic grain size number was 8 to 8.5 according to JIS in all the specimens. **Figs. 2** and **3** show the sectional distribution of hardness increment ΔHV near a surface after the nitriding for 20 and 40 s, respectively. Whereas the hardness increase was small and so was the effect of nitriding time with Steel A (0.016 mass% Ti), the hardness increase was larger with Steels B and C (0.025 and 0.046 mass%, respectively), exhibiting such sectional hardness distributions that the hardness increased near the surface only. The largest maximum hardness was obtained with Steel C, followed by B and then A: the maximum hardness increased with the Ti content. Comparing Figs. 2 and 3, one sees that as the nitriding time increases the depth of the hardened layer increases, but the change in maximum hardness is small.

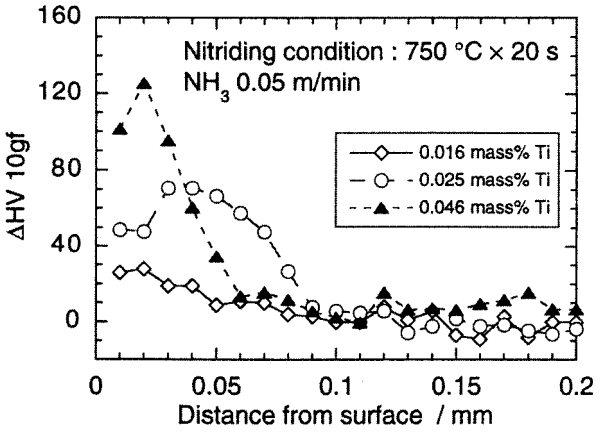

Fig. 2 Influence of Ti content on hardness distributions in the cross section of sample (nitriding condition: 750°C × 20s, NH_3 0.05 m/min)

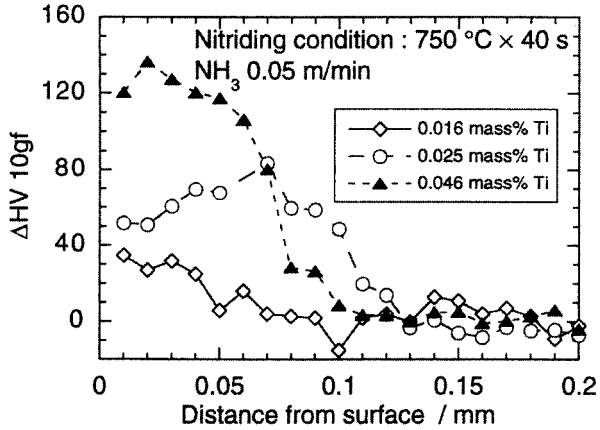

Fig. 3 Influence of Ti content on hardness distributions in the cross section of sample (nitriding condition: 750°C × 40s, NH_3 0.05 m/min)

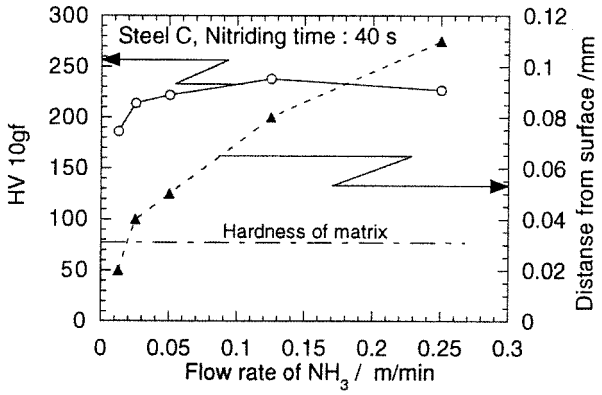

Fig. 4 Influence of flow rate of NH_3 on hardening behavior (maximum hardness and thickness of hardened layer)

Fig. 4 shows the influence of the NH_3 flow rate on the hardness of Steel C. The solid line shows the hardness (left-side scale) just before the rapid fall of hardness at the diffusion front of N, and the dotted line the distance from the surface to the points of measurement (right-side scale). While hardness was not affected by the NH_3 flow rate significantly, the thickness of the hardened layer increased as the flow rate increased.

The above results made it clear that in short-time nitriding, the maximum hardness near a surface was determined principally by the Ti content in steel and the thickness of the hardened layer was affected significantly by the factors that determined the amount of nitriding, namely nitriding time and the NH_3 flow rate.

3.2 Observation of precipitates

To study the mechanism of strengthening, the authors observed the precipitates forming through nitriding using the specimens of Steels C and D.

Fig. 5 shows the results of observation of a surface layer and a center portion by the replica method. Although coarse TiS particles approximately 0.03 to 0.2 μm in size were found both in the surface layer and center portion, their distribution density was low. Since the TiS particles were found not only in the surface layer but also in the center portion, they were judged to have formed during the production processes of the steel sheets, and not to be directly related to the precipitation during the nitriding.

Next, the authors observed the internal structure of Steels C and D with the thin film specimens prepared through the electrolytic polishing. The coarse precipitates as those found in the replica observation were observed also in a low density in the center portion, but no fine precipitates other than coarse ones were found in observations from any crystal orientations. As typical examples of the observation, **Fig. 6** shows a bright field image and an electron beam diffraction pattern, both taken at a center portion with the incident electron beam in the <110> orientation. The contrasts in the bright field image of Fig. 6 (a) are bend contours, which appear depending on the Bragg condition. They appear more conspicuously at these positions when there are fine precipitates, but there are no such precipitates here. On the other hand, in the hardened surface layer, the authors found ultra-fine tabular precipitates as shown with the bright field image and the electron beam diffraction pattern in **Fig. 7**. The precipitates were observed clearly only when the incident electron beam was set in the <001> orientation so that the {200} plane of

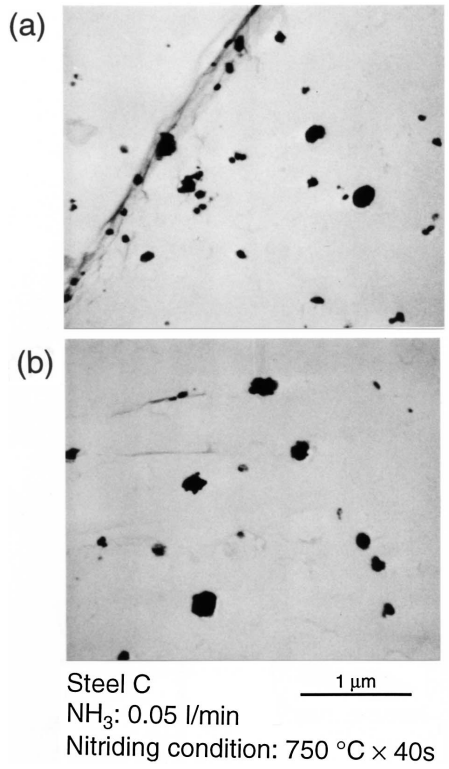

Fig. 5 Transmission electron micrographs of precipitates observed by the replica method
(a) The surface hardened layer, (b) the central layer

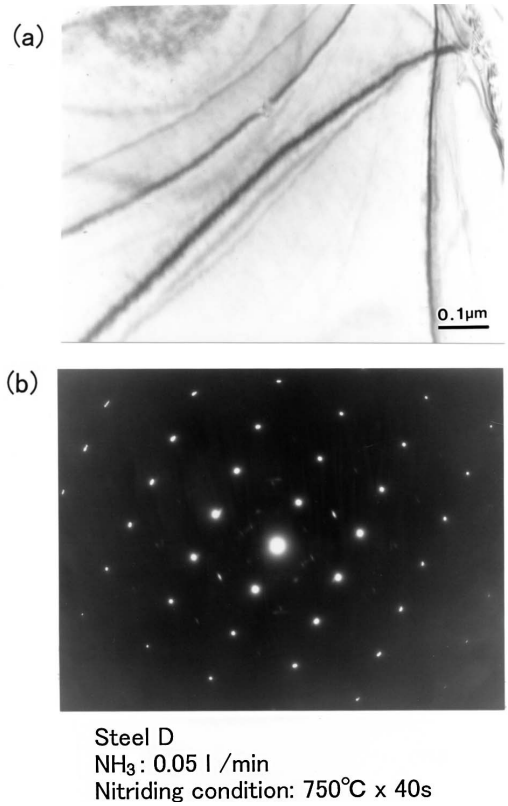

Fig. 6 Transmission electron micrographs showing a microstructure in the central part of the sample
(a) Bright field image, (b) Selected area diffraction pattern

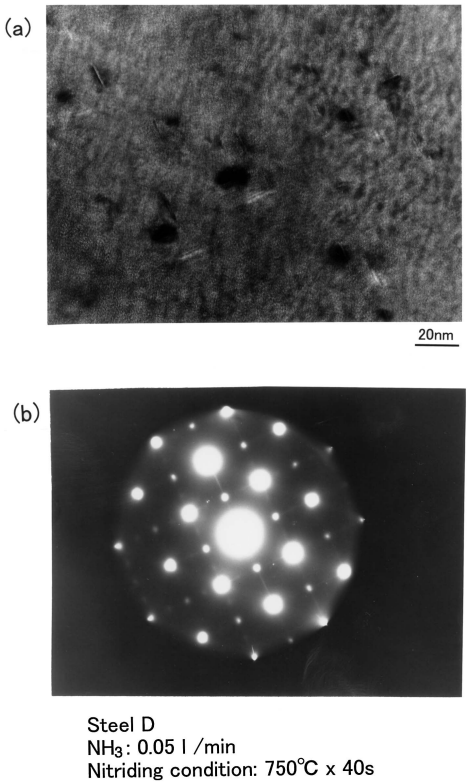

Fig. 7 Transmission electron micrographs showing fine precipitates observed in the surface hardened layer
(a) Bright field image, (b) Selected area diffraction pattern

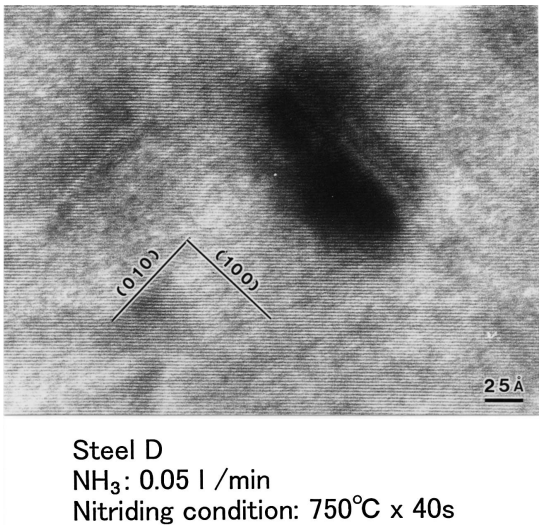

Fig. 8 High-resolution transmission electron micrograph of lattice image of fine precipitates. Incident electron beam direction is parallel to <001> direction.

iron was parallel to the electron beam.

To clarify the shape of the tabular precipitates in more detail, the authors observed them with high-resolution TEM images obtained with the electron beam in the same orientation. **Fig. 8** shows a lattice image of one of the tabular precipitates. Judging from the fine horizontal stripes, which are the (110) planes of iron, the precipitate has a very thin tabular shape at it sits on the (100) and (010) planes at

an angle of 45°. There are streaks stretching in the <100> orientation in the electron beam diffraction pattern of Fig. 7(b); they stretch in the thickness direction of the tabular precipitate, and indicate that the precipitate is very thin. Form Figs. 7 and 8, the precipitate was estimated to be several atom layers thick and approximately 10 nm across. The fact that the fine tabular precipitates were found only in the surface layers hardened by nitriding indicates the possibility that they are precipitates of Ti nitride or fine clusters containing Ti and N. Thus the formation of the fine precipitates or clusters is presumed to be the cause of the hardening of the surface layers.

4. Discussion

4.1 Nitrogen diffusion and precipitation behavior of TiN at nitriding of Ti-containing steel

The test results showed that nitriding treatment of Ti-containing steels resulted in hardening only of surface layers. The results also indicated that the hardening of the surface layers resulted most probably from the precipitation of TiN in fine particles. In view of the results, the authors estimated the precipitation behavior of TiN by calculation taking into consideration the diffusion of N from the surfaces to the inside of a steel material. A model was constructed for the calculation under the following assumptions and preconditions:

(1) Nitrogen introduced into steel by nitriding diffuses towards the inside, forming TiN.
(2) TiN is assumed to be the only nitride that forms: the formation of AlN is disregarded.
(3) The value of Ti* defined earlier is used as the amount of Ti that combines with N during nitriding.
(4) The classical nucleation theory applies to the nucleation of TiN.
(5) Local equilibrium is maintained at the precipitate/matrix interface during the nucleation and growth of TiN precipitates.
(6) The rate of the TiN precipitation is determined by the diffusion of Ti, and the N distribution near a precipitate particle is approximated under the condition of constant activity.
(7) Sheet thickness is divided equally into n sections each Δx in thickness, the N concentration C_N in each of the sections x is calculated by the calculus of finite differences. Then, assuming that the N concentration C_N in each of the sections obtained through the above calculation is the average in the section, the precipitation of TiN is calculated. Finally, the distribution of solute N is calculated by subtracting N as TiN from C_N .
(8) In calculating the TiN precipitation in each of the thickness sections, the concentration gradient of Ti at the interface of a precipitate, which is necessary for calculating the influx of Ti into the precipitate, is obtained not by directly calculating the distribution of Ti concentration near the precipitate but by using Zener's stationary solution [3, 4], which is

$$\left.\frac{\partial C_{Ti}}{\partial r}\right|_{r=R} = \frac{C_{Ti}^{\infty} - {}^{b}C_{Ti}}{R} \qquad (1)$$

where R is the radius of a precipitate, r is the distance from the precipitate center, ${}^{b}C_{Ti}$ is the Ti concentration on the matrix side of the precipitate/matrix interface. Here, the average Ti concentration C_{Ti} in Δx is used as the value of C_{Ti}^{∞}, which is the Ti concentration at an infinite distance. This calculating technique makes it possible to approximate the TiN precipitation amount without considering microscopic unevenness of concentration of the elements even when the nucleation occurs at any time.

The diffusion of N was calculated by solving the following diffusion equation:

$$\frac{\partial C_N}{\partial t} = D_N \frac{\partial^2 C_N}{\partial x^2} \qquad (2)$$

where D_N is the diffusion coefficient of N in α-iron, C_N is the N concentration, and t is time. The initial condition is set as $C_N = C_{N0}$ at a surface and $C_N = 0$ in the inside. Here, C_{N0} means the N concentration determined by the potential of N at a surface. On the other hand, the boundary condition is set as $C_N = C_{N0}$ at a surface and ${}^{d}C_N / dx = 0$ at the thickness center.

Next, the nucleation of TiN was calculated. The frequency of nucleation I was calculated using the equation below on an assumption that the classical nucleation theory applied to the nucleation of TiN. Here, the incubation period was taken into consideration applying the approximation method proposed by Akamatsu et al. [5].

$$\begin{aligned} I &= (\rho / \alpha^3)\, D_{Ti}\, {}^{b}x_{Ti} \exp\left(-\Delta G^* / R_g T\right)(h_g / h_1) \\ \Delta G^* &= 16\pi\sigma^3 / \left\{3\,(\Delta G / V_{TiN})^2\right\} \\ \Delta G &= 0.5 R_g T \log\left[({}^{a}x_{Ti}\, {}^{a}x_N) / ({}^{b}x_{Ti}\, {}^{b}x_N)\right] \\ h_g &= \sqrt{2 D_{Ti}\, t} \\ h_1 &= r^*\left[(V_\alpha / V_{TiN})(1/ x_{Ti})\right]^{1/3} \end{aligned} \qquad (3)$$

where ρ is dislocation density, which is given as $\rho = 1.0 \times 10^{12}\,\mathrm{m}^{-2}$, α is the lattice constant of the matrix, σ is the surface energy between the matrix and TiN, T is temperature, ΔG^* is activation energy, ΔG is the change in chemical energy when 1 mol of TiN forms, V_{TiN} is the molar volume of TiN, V_α is the molar volume of iron, R_g is the gas constant (J/mol/K), D_{Ti} is the diffusion coefficient of Ti in iron, ${}^{a}x_{Ti}$ and ${}^{a}x_N$ are the mean molar concentrations of Ti and N, respectively, in x, ${}^{b}x_{Ti}$ and ${}^{b}x_N$ are the molar concentrations of Ti and N, respectively, on the matrix side of the TiN/matrix interface, and r^* is the critical nuclear radius of a precipitate. The value of σ was assumed to change from 0.01 to 0.3 J/mol. This is because the authors thought that the coherence of a precipitate with the matrix would change depending on the precipitate size, and as a consequence, the surface energy would change [6].

On the other hand, the precipitate growth was calculated from the mass balance between the amount of Ti influx into a precipitate and the growth of the precipitate using the following equation:

$$\frac{dR}{dt}\left[{}^{TiN}y_{Ti}\,(V_\alpha / V_{TiN}) - {}^{b}x_{Ti}\right] = -D_{Ti}\,({}^{a}x_{Ti} - {}^{b}x_{Ti})/R \qquad (4)$$

where ${}^{TiN}y_{Ti}$ is the atom fraction of Ti among the lattice positions of TiN to be occupied by Ti, which is equal to 1. In consideration of the fact that the diffusion of N is far faster than that of Ti, and as a result, the activity of N is constant at any position, the distributions of the Ti and N concentrations near a precipitate ${}^{b}x_{Ti}$, ${}^{b}x_N$ used in the above calculations can be obtained in a ternary isothermal phase diagram of a Fe-Ti-N system as the components of Ti and N at the point where the equi-activity curve of N that passes through ${}^{a}x_{Ti}$ and ${}^{a}x_N$ intersects a solubility product curve [7].

The method of calculation was as follows. First, Equation (2) was solved by the calculus of finite differences under the condition that time interval Δt was less than $0.5\Delta x^2/D_N$. The distribution of solute N after the TiN precipitation was calculated by estimating the amounts of Ti and N consumed during a time period Δt by the nucleation of new precipitates and the growth of already existing precipitates and subtracting the values thus obtained from the amounts of Ti and N before the precipitation. The diffusion coefficients of Ti and N in iron D_{Ti}, D_N [8], the solubility product of TiN [9] and the activity of N α_N [10] that the authors used for the calculation are given below.

$$D_{Ti} = 6.8 \times 10^{-3} \exp\left(-26100 / R_g T\right) \quad [\mathrm{m^2/s}] \quad (5)$$

$$D_N = 1.13 \times 10^{-6} \exp\left[-83\left(1 - 14.03 / T\right) / R_g T\right] \quad [\mathrm{m^2/s}] \quad (6)$$

$$\log\left[Ti^*\right][N] = -16750 / T + 5.89 \quad (7)$$

$$\alpha_N = x_N \exp\left(x_{Ti} W_{TiN} / R_g T\right)$$
$$W_{TiN} = 483.86 - 1.13 \times 10^{-6} / T \quad (8)$$

The authors calculated the N diffusion from the surface to the inside and the TiN precipitation behavior using the above model and under the condition of the chemical composition of Steel C, a nitriding temperature of 750°C and a nitriding time of 40 s. From the amount of nitriding of the entire sheet, the N concentration at the surface was estimated to be 300 ppm, and this value was used for the calculation. **Fig. 9** shows the distribution of solute N in the thickness direction. For comparison purposes, the graph also shows the result of a calculation not considering the precipitation of TiN. **Fig. 10** shows the distribution of solute Ti in the thickness direction. While these graphs were obtained assuming $\sigma = 0.3$ J/mol, changing σ from 0.01 to 0.3 J/mol resulted in little change in the distributions of solute N and Ti. These results indicate that TiN precipitates near the surfaces, and the precipitation suppresses the diffusion of N toward the inside of the sheet. Whereas the concentration of solute Ti was nearly zero and the TiN precipitation came to an end in the portion to which N diffused, the TiN precipitation did not occur at all in the portion to which the N diffusion did not reach, which suggests that TiN precipitated rapidly at the front of the N diffusion.

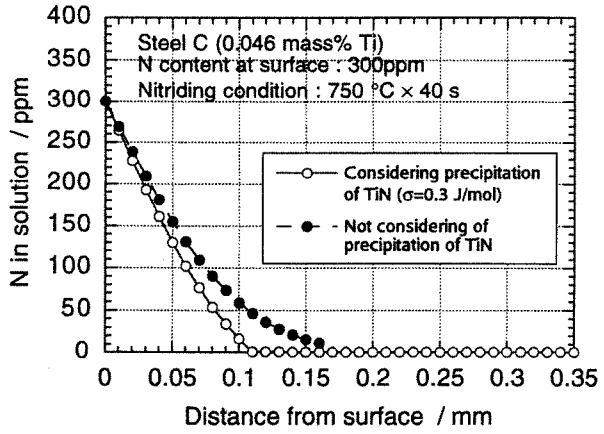

Fig. 9 Calculation result showing distributions of solute N

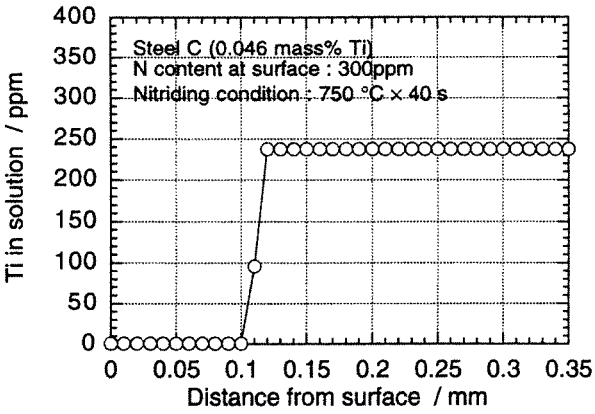

Fig. 10 Calculation result showing distributions of solute Ti

The above calculation results indicate that the TiN precipitation amount depends on the Ti addition amount, and in the portion to which N diffused, the TiN precipitation quickly comes to an end, having consumed all the solute N and Ti. Assuming that the main factor of the hardening of surface layers resulting from nitriding of a Ti-containing steel is the precipitation strengthening by TiN, the calculation result well explains the test result that the Ti addition amount determines the TiN precipitation amount and the hardness of the hardened layers. The calculation also showed that more TiN precipitated and the hardened portion expanded as the N diffusion advanced toward the inside of steel with time, which agreed well with the hardening behavior clarified through the tests.

4.2 Strengthening mechanism of surface layers by nitriding

Although the authors did not observe the changes in macroscopic structure such as crystal grain size, worked structure and transformation phases, they thought it highly probable that the mechanism of the hardening of surface layers involves solid-solution strengthening and precipitation strengthening. In the meantime, the authors measured by the internal friction method the amount of solute N using Steel C specimens that had been hardened to the thickness center through nitriding, and found that the solute N amount was approximately 5 ppm: thus it was found that the contribution of solute N to the strengthening was comparatively small. Therefore, the main factor of the hardening resulting from nitriding is presumed to be precipitation strengthening.

The increase in yield stress resulting from precipitation strengthening is expressed according to the Ashby-Orowan equation[11] as follows:

$$\Delta\tau_y = 0.84\left(1.2Gb / 2\pi L\right) 1\mathrm{n}\left(d / 2b\right) \quad (9)$$

where $\Delta\tau_y$ is the increment of yield shear stress, G is the modulus of rigidity of the matrix, which is G = 83,100 MPa[12], b is the Burgers vector, which is b = 0.25 nm, L is the distance between precipitate particles, and d is the mean diameter of particle sections intersected by a slip plane.

Here, letting n_s be the number of particles intersected by a unit area of a slip plane, the relationship between L and n_s is expressed as

$$L = n_s^{-1/2} \quad (10)$$

This equation has been obtained assuming that the particles are spherical. However, since the precipitates that the authors observed were tabular, they examined the applicability of the equation in such a case.

In the case where the precipitate particles are spherical having a radius of r, to begin with, n_s is equal to the number of particles in a parallelepiped including a slip plane and having a height of $2r$, as shown in **Fig. 11**(a). Letting f be the volume fraction of a particle and n_v the number of particles per unit volume, f is given as the product of n_v and the volume of a particle. Accordingly, n_v and n_s are given as follows[13]:

$$n_v = 3f / 4\pi r^3 \quad (11)$$

$$n_s = 2rn_v = 3f / 2\pi r^2 \quad (12)$$

Next, the equations to calculate n_v and n_s are defined for the case where the precipitate particles are tabular, or disc-shaped. Letting r be the radius of a disc-shaped particle, t its thickness and θ the angle

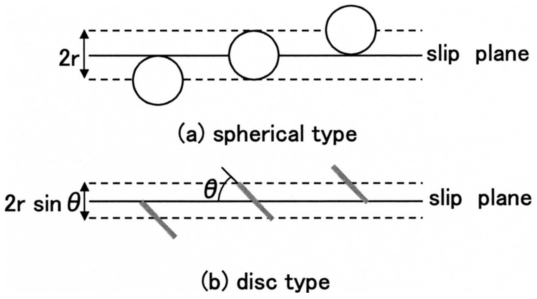

Fig. 11 The number of particles intersected per unit area of slip plane

between a slip plane and the plane of the particle, the volume of a particle is $\pi r^2 t$, and n_s is equal to the number of particles in a parallelepiped including a slip plane and having a height of $2r\sin\theta$, as shown in Fig. 11(b). Accordingly, n_v and n_s are given as follows:

$$n_v = f / \pi r^2 t \quad (13)$$

$$n_s = 2r\sin\theta\, n_v = 2f\sin\theta / \pi r t \quad (14)$$

Since the particles precipitated on the {100} plane in the present test and the slip plane of the matrix was the {110} plane, θ is equal to 45°.

Further, in the case where the particles are spherical, letting D represent the real diameter of a precipitate, the mean diameter x of particle sections intersected by a slip plane is equal to the diameter of a cylinder having a height of X and a volume equal to that of a sphere that has a diameter of D, and thus it is given as [14)]

$$x = (2/3)^{1/2} D = 0.816D \quad (15)$$

In the case where the particles are tabular, on the other hand, x is equal to the height of a rectangle having a width of D and an area equal to that of a circle that has a diameter of D, and thus it is given as

$$x = (\pi/4)\, D = 0.785D \quad (16)$$

Using the above equation, the authors calculated the volume fraction f of TiN on an assumption that Ti in the portions to which nitrogen had diffused would precipitate as TiN stoichiometrically, and based on this, they calculated the increment of yield stress $\Delta\sigma_y$. The result is shown in **Fig. 12**. Here, $\Delta\sigma_y$ was assumed to be equal to $2\Delta\tau_y$, and from observation results, the disc-shaped precipitate to be 10 nm in diameter and 0.3 nm in thickness. The graph also shows the increment of strength estimated from the test results. The estimation was done on the assumptions that Ti* < 0 and that strength in terms of MPa was three times as large as hardness in terms of HV, and using as a reference the maximum hardness of Steel A, the hardness increase of which was considered to be free from the influence of Ti. The calculated strength increment increased with Ti*, which agreed with the trend observed through the tests. While the calculation yielded a value closer to the measured value under the assumption of a tabular shape, there still remained a considerable difference. In view of this, the authors studied the cause of the difference as described below.

Since Equation (16) is a function of the diameter X and volume fraction f of the TiN precipitates, the volume fraction f was examined. According to Jack's report [15)], in an Fe-X-N alloy (X is Ti, V, Cr, Mn, Nb, Mo, Ta or W), the precipitation of carbonitride from a supersaturated solid solution proceeds from the formation of GP-

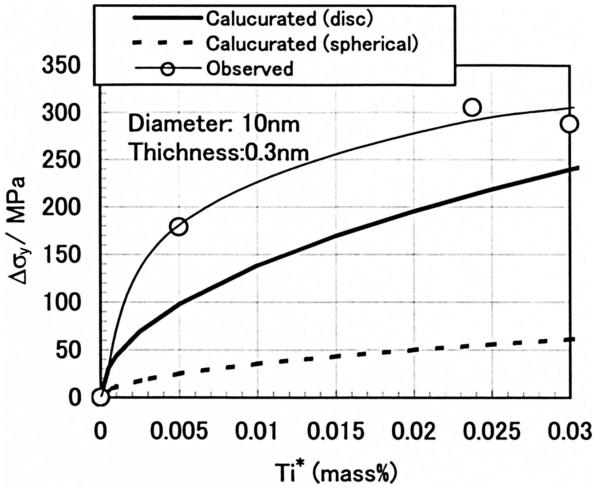

Fig. 12 Dependence of $\Delta\sigma_y$ on Ti* content. Comparison of calculated result and values estimated by measured hardness.

zone-like clusters in the initial stage to the growth from metastable precipitate to stable precipitate. The GP-zone-like clusters that form during the process have a layer wherein X atoms substitute for Fe, and N atoms exist at octahedral positions of bcc, forming an XN structure, and another layer wherein N atoms occupy the octahedral positions above and below the X atoms that substitute for Fe, forming an FeN structure. That is to say that the composition of an entire cluster is Fe_2XN_3. Stoichiometrically, such a cluster, if exists, exhibits three times as large a volume fraction as TiN normally does per unit amount of Ti. In this case, the calculated strength increment increases to 1.4 times the calculation result described earlier, closer to the test results. Therefore, if clusters as described above form, even partially, the difference between the calculated and measured strength increments will possibly decrease.

Such clusters, when formed, are expected to precipitate coherently with the matrix, and the coherence strain possibly results in a significant increase in strength.

While the main mechanism of the strengthening of hardened surface layers is considered from the above to be precipitation strengthening, in order to quantitatively examine the strength increment, it is necessary to observe the fine precipitates in more detail to clarify their component ratios and other characteristics.

5. Summary

This paper has studied the surface hardening of Ti-containing steel sheets through rapid nitriding and discussed the formation behavior of hardened layers near sheet surfaces and the mechanism of the strengthening. The essence of the results is summarized as follows:

(1) The surface layers of a Ti-containing steel sheet are strengthened through rapid nitriding.

(2) The maximum hardness near a surface obtained by the nitriding depends on the addition amount of Ti, and is influenced by nitriding time and the flow rate of NH_3 only to limited extents. On the other hand, the nitriding time and the flow rate of NH_3 determine the depth of the hardened layers.

(3) Electron microscope observation revealed tabular, or disc-shaped, particles several atom layers thick and approximately 10 nm across precipitating on the {100} plane in the hardened surface layers. The particles are possibly those of TiN precipitate or clusters con-

taining Ti and N.

(4) The behavior of TiN precipitation near sheet surfaces was estimated using a model of the diffusion of nitrogen in steel in consideration of the TiN precipitation. The result indicates that nitrogen forms TiN immediately after being introduced into the steel and it diffuses to farther inside as more of it is introduced and supersaturation is reached locally.

(5) While the principal mechanism of the strengthening of the hardened surface layers is presumed to be the precipitation strengthening by TiN, it is also likely that the formation of Fe-Ti-N clusters leads to the strength increase.

References

1) Iron & Steel Institute of Japan: Iron & Steel Handbook VI. 3rd Edition, Tokyo, Maruzen, 1982, p.568
2) Miura, M. et al.: CAMP-ISIJ. 7, 759(1994)
3) Zener, C.: J. Appl. Phys. 20, 950(1941)
4) Wert, C. et al.: J. Appl. Phys. 21, 5(1950)
5) Akamatsu, S. et al.: Tetsu-to-Hagané. 75, 993(1989)
6) Okamoto, T. et al.: Tetsu-to-Hagané. 84, 650(1998)
7) Akamatsu, S. et al.: Tetsu-to-Hagané. 78, 790(1992)
8) Japan Institute of Metals: Metals Data Book. 3rd Revised Edition, Tokyo, Maruzen, 1993
9) Akamatsu, S. et al.: ISIJ Int. 34, 9(1994)
10) Haerman, J. et al.: C. R. M. 59, 11(1982)
11) Gladman, T.: The Physical Metallurgy of Microalloyed Steels. The Institute of Materials, London,1997, p.52
12) Koda, S.: Introduction to Metal Physics. Revised Edition, Tokyo, Corona Publishing Co. Ltd., 1973, p.181
13) Tsusaki, K.: Latest Precipitate Control Metallurgy of Steel. Tokyo, Iron & Steel Institute of Japan, 2001, p.93
14) Gladman, T.: The Physical Metallurgy of Microalloyed Steels. The Institute of Materials, London, 1997, p.43
15) Jack, K.: Key Engineering Materials. 86-87, 1(1993)